Proceedings of BS2013:
13th Conference of International Building Performance Simulation Association, Chambéry, France, August 26-28

DEVELOPMENT OF A CONTROL-ORIENTED MODEL FOR BOREHOLE DYNAMICS FOR BUILDINGS EQUIPPED WITH GROUND COUPLED HEAT PUMPS

Ercan Atam, Clara Verhelst and Lieve Helsen
KU Leuven, Dep. of Mechanical Eng., Division of Applied Mechanics and Energy Conversion,
Celestijnenlaan 300A, BOX 2421, BE-3001 Leuven, Belgium,
{ercan.atam,clara.verhelst, lieve.helsen}@mech.kuleuven.be

ABSTRACT

This paper proposes to apply the celebrated Proper Orthogonal Decomposition (POD) approach in order to obtain a short-term control model for the temperature dynamics of the borehole system. The main idea behind POD-based modeling is the extraction of a set of optimal basis functions containing the main characteristics of the system from snapshots of the system dynamics at various time instants. This way, POD allows an accurate description of the heat diffusion process where the POD modes can be used as states of the control model. The obtained control model is used for control of heat extraction and injection.

INTRODUCTION

Energy prices resulting from increasing energy demand and decelerating supply has prompted substantial interest in clean and renewable energy in the last decades. Based on the fact that buildings account for approximately 40% of total energy use in Europe (EPBD, 2010) and similar percentages in the rest of the world, development of energy efficient buildings, heating and cooling technologies together with appropriate control strategies are required.

Ground coupled heat pump (GCHP) systems combined with low-exergy heat emission systems have the potential to reduce the primary energy use related to space heating and cooling by 70% compared to conventional heating and cooling systems. For GCHP systems with vertical borehole heat exchangers (BHE), however, the large investment cost of the borefield represents a major bottleneck. This explains the trend towards compact, hybrid GCHP systems which combine smaller boreholes with supplementary heating or cooling devices (Cullin, 2010). The control of such compact, hybrid GCHP systems constitutes an important and challenging problem both for academic and industrial communities (Scott and Amanda, 2011; Ridder et al., 2011).

Recent studies indicate the influence of the short-time response (Partenay et al., 2011; Yavuzturk and Spitler, 1999) and the control strategies used (Verhelst, 2012) on GCHP performances. For example, in hybrid GCHP systems when maximizing the share of the heat pump or passive cooling covering the heating and cooling loads, the fluid temperature should be respectively at the lower and upper optimal bound. Current rule-based control strategies fail to get optimal system operation within (but close to) the physical constraints. When operating near the temperature constraints, they often result in an on-off cycling, which is detrimental for both the system energy performance and installation life-time. To track a fluid temperature set-point without cycling, a closed-loop control strategy like Linear Quadratic Regulator (LQR) is appropriate. LQR requires a dynamic model of the system to be controlled. In this case, we need a BHE model to predict the response of the circulating fluid temperature to the injected or extracted heat power.

Most existing BHE models are however intended for simulation purpose and are far too complex to used in a control framework where a low-order linear state-space model form is desired (Kim et al., 2011). The first borehole control model, developed by Franke (Franke, 1998), was obtained by model reduction of the detailed DST-model in TRNSYS. Verhelst and Helsen (Verhelst and Helsen, 2011) evaluated two comparable methods: first, model reduction of a very simple first principle numerical model-which can be set up by hand and, second, parameter estimation of a resistance-capacitance model using TRNSYS simulation data. Monteyne et al. (Monteyne et al., 2011) evaluated the use of rational transfer functions in the variable $\sqrt{s}$ to describe the diffusion process, with the model parameters being identified from measurement data. These studies, dealing with the setup of a model predictive control (MPC) framework, aimed at obtaining a BHE model capturing both short and long term BHE dynamics. As a result, there is a tradeoff in these models in terms of accuracy when compared to a stand-alone short-term model or a stand-alone long-term model. Here, the focus is on modeling and control of the short-term BHE dynamics.

In this paper, we propose the Proper Orthogonal Decomposition (POD) method to obtain a reduced-order control model for short term LQR-based circulating fluid temperature control in a borehole. Compared to the standard model reduction techniques, POD allows us to focus on the fast dynamics in which we are interested. Compared to system identification, POD is a computationally less complex and physically more elegant technique, at least if a detailed numerical model is available. The current study can be extended to the more complex problem of borefiled control with hybrid GHP systems using more sophisticated control algorithms such as MPC.

TEMPERATURE DYNAMICS MODELING

The borehole filled with grout is shown in Figure 1 where an equivalent diameter approach is used. In the equivalent diameter approach the heat transfer from the U-tube is approximated by the heat transfer from a pipe with a hypothetical diameter through which the heat exchanging fluid circulates (Chiasson, 2007; Javed and Claesson, 2011). The system variables are listed in Table 1 at the end of the paper. The objective is the determination of the circulating fluid mean-value temperature over borehole length, $T_f(t)$, corresponding to an extracted/rejected heat per length, $q(t)$, and then the reverse problem of its control.

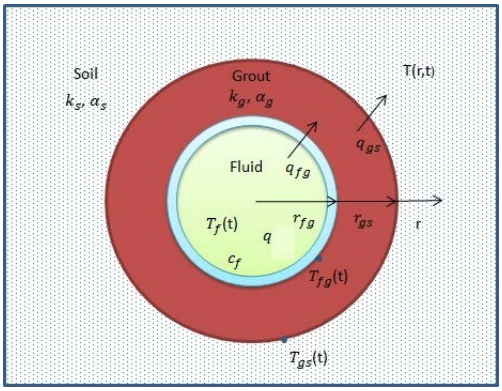

Figure 1: Borehole system.

For both the grout and the soil region the temperature distribution is modeled by

$$\frac{1}{\alpha(r)}\frac{\partial T}{\partial t} = \frac{1}{r}\frac{\partial}{\partial r}\left(r\frac{\partial T}{\partial r}\right), \qquad (1)$$

$$\alpha(r) = \begin{cases} \alpha_g, & \text{if } r_{fg} < r < r_{gs}, \\ \alpha_s, & \text{if } r > r_{gs}. \end{cases}$$

where α_g and α_s are grout and soil diffusivity, respectively. Assuming that the undisturbed initial ground temperature was $T(r,0) = T_0$, we can write $\lim_{r\to\infty} T(r,t) = T_0, \forall t$. However, assuming that at a sufficiently large radius $r = r_\star$ the effect of heat diffusion is negligible, we can approximate the above condition at infinity as

$$\left.\frac{\partial T(r,t)}{\partial r}\right|_{r_\star} = 0, \forall t.$$

The next step is to relate the fluid temperature $T_f(t)$ to the grout temperature $T_{fg}(t)$ at $r = r_{fg}$. Assume that a thermal resistance R_{fg} exists over the pipe periphery between the fluid in the pipe and the near outside grout. This thermal resistance takes into account the conduction resistance through the pipe and the fluid convective resistance (Chiasson, 2007; Javed and Claesson, 2011):

$$R_{fg} = \frac{1}{2\pi k_p}\ln\left(\frac{r_{p_i}}{r_{p_o}}\right) + \frac{1}{2\pi r_{fg} h_f}, \qquad (2)$$

where k_p is the pipe thermal conductivity, $r_{p_i} = r_{fg}, r_{p_o}$ are the inner and outer pipe radiuses, respectively, and h_f, is the fluid convective heat transfer coefficient. For short-time response analysis and considering for example variable flow rates, the value of h_f can change significantly between laminar and turbulent states but its effect on the T_f is small. The boundary condition between the circulating fluid and the grout is

$$T_f(t) - T_{fg}(t) = R_{fg} q_{fg}, \qquad (3)$$

where q_{fg} is the heat transfer at fluid-grout boundary and R_{fg} is the corresponding thermal resistance. Finally, the energy balance in the pipe results in

$$q = \pi r_{p_i}^2 \rho_f c_f \frac{dT_f}{dt} + q_{fg}, \qquad (4)$$

where c_f is the fluid specific heat and ρ_f is its density. Equation (4) is derived by assuming the fluid to be incompressible so that $\frac{du}{dT} = c_f$ and using the chain rule

$$\frac{du}{dt} = \frac{du}{dT_f}\frac{dT_f}{dt} = c_f\frac{dT_f}{dt},$$

where u denotes the specific internal energy. Next, we discretisize Equation (1) using n_g space nodes for the grout region and n_s nodes for the soil region as shown in Figure 2(a). Integration of Equation (1) over a control volume in Figure 2(c) and over a time step of size Δt gives

$$\underbrace{\int_t^{t+\Delta t}\left(\int_{\Delta V}\frac{1}{\alpha(r)}\frac{\partial T}{\partial t}dV\right)dt}_{S_1} = \underbrace{\int_t^{t+\Delta t}\left(\int_{\Delta V}\frac{1}{r}\frac{\partial}{\partial r}\left(r\frac{\partial T}{\partial r}\right)dV\right)dt}_{S_2}. \qquad (5)$$

Next, we will calculate the terms S_1 and S_2, starting with S_1. Changing the order of integration and using backward difference in time derivative approximation we obtain

$$S_1 = \int_{\Delta V}\left(\int_t^{t+\Delta t}\frac{1}{\alpha(r)}\frac{\partial T}{\partial t}dt\right)dV = \int_{\Delta V}\frac{1}{\alpha(r)}\left(T_P - T_{P^0}\right)dV, \qquad (6)$$

where T_P denotes the temperature at time $t + \Delta t$ and T_{P^0} at time t. Using $dV = 2\pi H r dr$, Equation (6) becomes

$$S_1 = \frac{\pi H r_e^2}{\alpha_e}\left(T_P - T_{P^0}\right) - \frac{\pi H r_w^2}{\alpha_w}\left(T_P - T_{P^0}\right), \qquad (7)$$

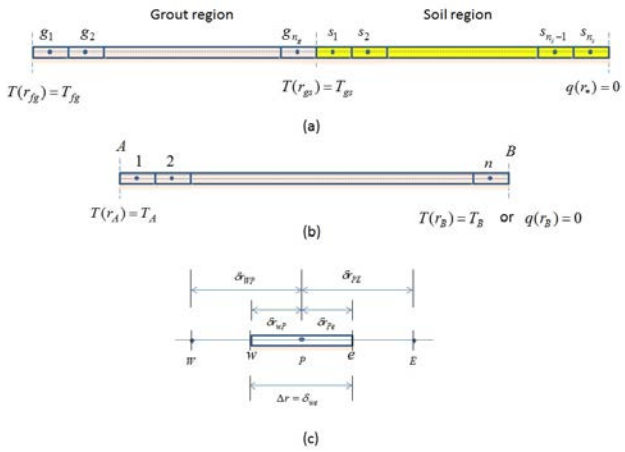

Figure 2: Borehole discrerization.

where H is the borehole length, w and e denote the west and east faces of an internal node P in Figure 2 (c). Now we will calculate S_2. Again, using $dV = 2\pi H r dr$, S_2 becomes

$$\begin{aligned} S_2 =& 2\pi H \int_t^{t+\Delta t} \left(\int_w^e \frac{\partial}{\partial r} \left(r \frac{\partial T}{\partial r} \right) dr \right) dt \\ =& 2\pi H \int_t^{t+\Delta t} \left[\left(r \frac{\partial T}{\partial r} \right)_e - \left(r \frac{\partial T}{\partial r} \right)_w \right] dt \\ =& 2\pi H \int_t^{t+\Delta t} \left[\left(r_e \frac{T_E - T_P}{\Delta r} \right) - \left(r_w \frac{T_P - T_W}{\Delta r} \right) \right] dt \\ =& \frac{2\pi H \Delta t}{\Delta r} \Big[r_e (T_E - T_P) - r_w (T_P - T_W) \Big], \end{aligned} \quad (8)$$

where the last equality is obtained using a fully implicit scheme (taking the temperatures in the time interval equal to the values at the end of the interval). Setting $S_1 = S_2$ we obtain

$$a_P T_P = a_W T_W + a_E T_E + a_{P^0} T_{P^0}, \quad (9)$$

where

$$\begin{aligned} a_P &= \frac{r_e^2}{\alpha_e} - \frac{r_w^2}{\alpha_w} + 2\frac{\Delta t}{\Delta r}(r_w + r_e),\ a_W = \frac{2\Delta t}{\Delta r} r_w, \\ a_E &= \frac{2\Delta t}{\Delta r} r_e,\ a_{P^0} = \frac{r_e^2}{\alpha_e} - \frac{r_w^2}{\alpha_w}. \end{aligned} \quad (10)$$

Equation (9) is for a general internal node P having the neighbor nodes W and E. Nodes with boundary faces need special treatment. Next, we will handle different boundary conditions which are required to derive the overall grout-soil discretization equations.

Case 1: $T(r_A) = T_A$**,**$T(r_B) = T_B$

For the first node with west face at r_A in Figure 2(b), we have

$$\begin{aligned} S_1 = 2\pi H \int_A^e \frac{1}{\alpha(r)} (T_P - T_{P^0}) r dr = \\ \frac{\pi H}{\alpha_e} r_e^2 (T_P - T_{P^0}) - \frac{\pi H}{\alpha_A} r_A^2 (T_P - T_{P^0}). \end{aligned}$$

We have

$$\begin{aligned} S_2 =& 2\pi H \int_t^{t+\Delta t} \left(\int_A^e \frac{\partial}{\partial r} \left(r \frac{\partial T}{\partial r} \right) dr \right) dt \\ =& 2\pi H \int_t^{t+\Delta t} \left[\left(r \frac{\partial T}{\partial r} \right)_e - \left(r \frac{\partial T}{\partial r} \right)_A \right] dt \\ =& 2\pi H \int_t^{t+\Delta t} \left[r_e \frac{T_E - T_P}{\Delta r} - r_A \frac{T_P - T_A}{\Delta r/2} \right] dt \\ =& \frac{2\pi H \Delta t}{\Delta r} r_e (T_E - T_P) - \frac{4\pi H \Delta t}{\Delta r} r_A (T_P - T_A). \end{aligned}$$

Setting $S_1 = S_2$, we get

$$a_P T_P = a_W T_W + a_E T_E + a_{P^0} T_{P^0} + a_A T_A \quad (11)$$

where

$$\begin{aligned} a_P &= \frac{r_e^2}{\alpha_e} - \frac{r_A^2}{\alpha_A} + 2\frac{\Delta t}{\Delta r}(2r_A + r_e),\ a_W = 0, \\ a_E &= \frac{2\Delta t}{\Delta r} r_e,\ a_{P^0} = \frac{r_e^2}{\alpha_e} - \frac{r_A^2}{\alpha_A},\ a_A = \frac{4\Delta t}{\Delta r} r_A. \end{aligned} \quad (12)$$

For any internal node in Figure 2(b), we have the Equations (9) and (10) repeated below:

$$a_P T_P = a_W T_W + a_E T_E + a_{P^0} T_{P^0}, \quad (13)$$

where

$$\begin{aligned} a_P &= \frac{r_e^2}{\alpha_e} - \frac{r_w^2}{\alpha_w} + 2\frac{\Delta t}{\Delta r}(r_w + r_e),\ a_W = \frac{2\Delta t}{\Delta r} r_w, \\ a_E &= \frac{2\Delta t}{\Delta r} r_e,\ a_{P^0} = \frac{r_e^2}{\alpha_e} - \frac{r_w^2}{\alpha_w}. \end{aligned} \quad (14)$$

For the last node with east face at r_B in Figure 2(b), we have

$$\begin{aligned} S_1 = 2\pi H \int_w^B \frac{1}{\alpha(r)} (T_P - T_{P^0}) r dr \\ = \frac{\pi H}{\alpha_B} r_B^2 (T_P - T_{P^0}) - \frac{\pi H}{\alpha_w} r_w^2 (T_P - T_{P^0}). \end{aligned}$$

Next, we obtain S_2 as

$$\begin{aligned}S_2 =&2\pi H\int_t^{t+\Delta t}\left(\int_w^B\frac{\partial}{\partial r}\left(r\frac{\partial T}{\partial r}\right)dr\right)dt\\ =&2\pi H\int_t^{t+\Delta t}\left[\left(r\frac{\partial T}{\partial r}\right)_B-\left(r\frac{\partial T}{\partial r}\right)_w\right]dt\\ =&2\pi H\int_t^{t+\Delta t}\left[r_B\frac{T_B-T_P}{\Delta r/2}-r_w\frac{T_P-T_W}{\Delta r}\right]dt\\ =&\frac{4\pi H\Delta t}{\Delta r}r_B(T_B-T_P)-\frac{2\pi H\Delta t}{\Delta r}r_w(T_P-T_W).\end{aligned}$$

Setting $S_1 = S_2$, we get

$$a_PT_P = a_WT_W + a_ET_E + a_{P^0}T_{P^0} + a_BT_B, \quad (15)$$

where

$$a_P = \frac{r_B^2}{\alpha_B}-\frac{r_w^2}{\alpha_w}+\frac{4\Delta t}{\Delta r}r_B+\frac{2\Delta t}{\Delta r}r_w,\ a_W=\frac{2\Delta t}{\Delta r}r_w,$$
$$a_E=0,\ a_{P^0}=\frac{r_B^2}{\alpha_B}-\frac{r_w^2}{\alpha_w},\ a_B=\frac{4\Delta t}{\Delta r}r_B. \quad (16)$$

Case 2: $T(r_A) = T_A$**,** $q(r_B) = 0$

The equations for the first node and for the internal nodes are the same as Equations (11)-(12) and (13)-(14), respectively. For the node with east face at r_B, we have

$$\begin{aligned}S_1 &= 2\pi H\int_w^B\frac{1}{\alpha(r)}(T_P-T_{P^0})rdr\\ &=\frac{\pi H}{\alpha_B}r_B^2(T_P-T_{P^0})-\frac{\pi H}{\alpha_w}r_w^2(T_P-T_{P^0}).\end{aligned}$$

Next, we obtain S_2 as

$$\begin{aligned}S_2 =&2\pi H\int_t^{t+\Delta t}\left(\int_w^B\frac{\partial}{\partial r}\left(r\frac{\partial T}{\partial r}\right)dr\right)dt\\ =&2\pi H\int_t^{t+\Delta t}\left[\left(r\frac{\partial T}{\partial r}\right)_B-\left(r\frac{\partial T}{\partial r}\right)_w\right]dt\\ =&2\pi H\int_t^{t+\Delta t}\left[0-r_w\frac{T_P-T_W}{\Delta r}\right]dt\\ =&-\frac{2\pi H\Delta t}{\Delta r}r_w(T_P-T_W).\end{aligned}$$

Setting $S_1 = S_2$, we get

$$a_PT_P = a_WT_W + a_ET_E + a_{P^0}T_{P^0}, \quad (17)$$

where

$$a_P = \frac{r_B^2}{\alpha_B}-\frac{r_w^2}{\alpha_w}+\frac{2\Delta t}{\Delta r}r_w,\ a_W=\frac{2\Delta t}{\Delta r}r_w,$$
$$a_E=0,\ a_{P^0}=\frac{r_B^2}{\alpha_B}-\frac{r_w^2}{\alpha_w}. \quad (18)$$

Temperature dynamics for combined grout-soil region

Using Equations (11)-(12), (13)-(14) and (15)-(16) in Section with $\alpha_e = \alpha_A = \alpha_w = \alpha_B = \alpha_g$, $r_A = r_{fg}$, $T_A = T_{fg}, r_B = r_{gs}$, $T_B = T_{gs}$, $\Delta r = (\Delta r)_g$, we get

$$x_g(k+1) = A_gx_g(k) + B_g\begin{pmatrix}T_{fg}(k)\\ T_{gs}(k)\end{pmatrix}, \quad (19)$$

where $x_g \triangleq [T_{g_1}\cdots T_{g_{n_g}}]^T$. In the same way, using Equations (11)-(12), (13)-(14) and (17)-(18) in Section with $\alpha_e = \alpha_A = \alpha_w = \alpha_B = \alpha_s$, $r_A = r_{gs}$, $T_A = T_{gs}, r_B = r_\star$, $q_B = 0$, $\Delta r = (\Delta r)_s$, we get

$$x_s(k+1) = A_sx_s(k) + B_sT_{gs}(k), \quad (20)$$

where $x_s \triangleq [T_{s_1}\cdots T_{s_{n_s}}]^T$. From the continuity of heat flux at $r = r_{gs}$, we have

$$-k_g\frac{T_{gs}-T_{g_{n_g}}}{(\Delta r)_g/2} = -k_g\frac{T_{s_1}-T_{gs}}{(\Delta r)_s/2},$$

which when combined with $T_{g_{n_g}} = C_{g_{n_g}}x_g$ and $T_{s_1} = C_{s_1}x_s$, where $C_{g_{n_g}} = [0\ 0\cdots 1]^T \in \mathbb{R}^{n_g}, C_{s_1} = [1\ 0\cdots 0]^T \in \mathbb{R}^{n_s}$, gives

$$T_{gs} = \frac{k_g(\Delta r)_sC_{g_{n_g}}x_g + k_s(\Delta r)_gC_{s_1}x_s}{k_g(\Delta r)_s + k_s(\Delta r)_g}. \quad (21)$$

Using Equation (21) in Equations (19) and (20), partitioning B_g as $B_g = [B_g^1 \quad B_g^2]$ and defining $x \triangleq [x_g\ x_s]^T$, we obtain the combined grout-soil temperature dynamics as in (22) at the top of page 5.

Mean-value temperature prediction of the circulating fluid

In addition to Equation (3), we can write another expression for q_{fg} as

$$q_{fg} = -k_g\frac{A}{L}\frac{dT}{dr}\bigg|_{r=r_{fg}} \cong -4\pi k_gr_{fg}\frac{T_{g_1}-T_{fg}}{(\Delta r)_g}. \quad (23)$$

Using Equations (3) and (23), we obtain

$$\begin{aligned}T_{fg} =&\frac{1}{1+k_{fg}}T_f+\frac{k_{fg}}{1+k_{fg}}T_{g_1}\\ =&\frac{1}{1+k_{fg}}T_f+\frac{k_{fg}}{1+k_{fg}}C_{g_1}x, \quad (24)\end{aligned}$$

where the temperature at the first grout node, T_{g_1}, is expressed as $T_{g_1} = C_{g_1}x$ with $C_{g_1} = [1\,0\cdots 0]^T \in \mathbb{R}^{n_g+n_s}$ and

$$k_{fg} = \frac{4\pi k_gR_{fg}r_{fg}}{(\Delta r)_g}.$$

Using Equation (24), Equation (22) becomes

$$x(k+1) = \left[A+\frac{k_{fg}}{1+k_{fg}}BC_{g_1}\right]x(k)+\frac{1}{1+k_{fg}}BT_f. \quad (25)$$

Now, using Equation (24) in Equation (3) we get

$$q_{fg} = \frac{\frac{k_{fg}}{1+k_{fg}}(T_f - C_{g_1}x)}{R_{fg}}. \quad (26)$$

$$x(k+1) = \left[\begin{array}{c:c} A_g + \dfrac{k_g(\Delta r)_s}{k_g(\Delta r)_s + k_s(\Delta r)_g} B_g^2 C_{g_{n_g}} & \dfrac{k_s(\Delta r)_g}{k_g(\Delta r)_s + k_s(\Delta r)_g} B_g^2 C_{s_1} \\ \hdashline \dfrac{k_g(\Delta r)_s}{k_g(\Delta r)_s + k_s(\Delta r)_g} B_s C_{g_{n_g}} & A_s + \dfrac{k_s(\Delta r)_g}{k_g(\Delta r)_s + k_s(\Delta r)_g} B_s C_{s_1} \end{array}\right] x(k) + B_g^1 T_{fg}(k)$$
$$\triangleq Ax(k) + BT_{fg}(k). \tag{22}$$

$$x_{sys}(k+1) = \left[\begin{array}{c:c} 1 - \dfrac{\Delta t k_{fg}}{(1+k_{fg}) R_{fg} (2\pi r_{p_i}^2 \rho_f c_f)} & \dfrac{\Delta t k_{fg}}{(1+k_{fg}) R_{fg} (2\pi r_{p_i}^2 \rho_f c_f)} C_{g_1} \\ \hdashline \dfrac{1}{1+k_{fg}} B & A + \dfrac{k_{fg}}{1+k_{fg}} B C_{g_1} \end{array}\right] x_{sys}(k) + \frac{\Delta t}{2\pi r_{p_i}^2 \rho_f c_f} u(k),$$

$$\triangleq A_{sys} x_{sys}(k) + B_{sys} u(k),\ y = T_f = [1\, 0 \cdots 0] x_{sys} \triangleq C_{sys} x_{sys}. \tag{28}$$

Using expression Equation (26) and discretisizing (4) (with the same time discretization step size Δt) we get

$$T_f(k+1) = \left[1 - \frac{\Delta t k_{fg}}{(1+k_{fg}) R_{fg} (2\pi r_{p_i}^2 \rho_f c_f)}\right] T_f(k) + \frac{\Delta t k_{fg}}{(1+k_{fg}) R_{fg} (2\pi r_{p_i}^2 \rho_f c_f)} C_{g_1} x + \frac{\Delta t}{2\pi r_{p_i}^2 \rho_f c_f} u, \tag{27}$$

where $u = q$. Finally, letting $x_{sys} = [T_f\ x]^T$, we can write the combined system of Equation (27) and (25) as in Equation (28) at the top of page 5.

POD-BASED MODEL REDUCTION

In this section we will give a summary of the model reduction problem by POD and its solution. The interested reader is referred to (Holmes et al., 1996) for details. Let $\mathcal{H}$ be an N-dimensional Hilbert space with an orthonormal basis $\{f_i\}_{i\in\mathbb{I}}$ where $\mathbb{I} = \{1, 2, \cdots, N\}$. Let $\mathcal{H}_1$ and $\mathcal{H}_2$ be a complemnetary orthogonal decomposition of $\mathcal{H}$ with the corresponding basis functions $\{f_i\}_{i\in\mathbb{I}_1}$ and $\{f_i\}_{i\in\mathbb{I}_2}$, respectively. Any element $f \in \mathcal{H}$ can be written as

$$f = \sum_{i\in\mathbb{I}_1} a_i f_i + \sum_{i\in\mathbb{I}_2} a_i f_i = f_1 + f_2, \tag{29}$$

where the coefficients $a_i =< f, f_i >$ are the Fourier coefficients. This decomposition has the following properties:

- $||f - f_1||^2 = ||f_2||^2 = \sum_{i\in\mathbb{I}_2} a_i^2$,
- $||f - f_2||^2 = ||f_1||^2 = \sum_{i\in\mathbb{I}_1} a_i^2$,
- $f_1 = \arg\min_{f_0\in\mathcal{H}_1} ||f - f_0||$,
- $f_2 = \arg\min_{f_0\in\mathcal{H}_2} ||f - f_0||$,

where $||\cdot||$ is the inner product-induced norm. The geometric meaning of the last two properties is that f_1 is the best approximation of f in $\mathcal{H}_1$ and f_2 is that of f in $\mathcal{H}_2$. The objective is the "optimal" projection of f onto $\mathcal{H}_1$. For that, first an order complexity function $c_o : \mathcal{H} \to \mathbb{Z}_+$ is defined as the number of nonzero Fourier coefficients in Equation (29). Next, we define the misfit function $d_{mf} : \mathcal{H} \times \mathcal{H}_1 \to \mathbb{R}_+$ as $d_{mf}(f, f_1) \triangleq ||f - f_1||$. Then, the optimal projection problem can be stated as follows: *given $f \in \mathcal{H}$ of complexity order $c_o(f)$, find $f_1 \in \mathcal{H}_1$ with complexity order $c_o(f_1) \le c_o(f)$ such that $d_{mf}(f, f_1)$ is minimal*. The solution of this problem is as follows. If the Fourier coefficients $\{a_1, a_2, \cdots a_N\}$ are ordered as

$$a_{i_1}^2 \ge a_{i_2}^2 \ge \cdots \ge a_{i_{c_o(f_1)}}^2 \ge \cdots \ge a_{i_N}^2,$$

then the optimal projection f_1 onto $\mathcal{H}_1$ is given as

$$\hat{f}_1 = \sum_{j=1}^{c_o(f_1)} a_{i_j} f_{i_j}, \tag{30}$$

where hat denotes the projection and

$$d_{mf}(f, f_1) = \sum_{j=c_o(f_1)+1}^{N} a_{i_j}^2.$$

So far we considered the optimal projection of a single vector $f \in \mathcal{H}$ onto $\mathcal{H}_1$. Next, we will consider the extended problem of optimal projection of a set of

vectors onto $\mathcal{H}_1$. To deal with this kind of problem, let

$$F_{snap} = \Big[f(t_1) \quad f(t_2) \cdots \quad f(t_n) \Big],$$

where $f(t_i) \in \mathcal{H}, t_i \in \mathbb{T}, i = 1 : n$ and $\mathbb{T}$ is a time interval. For each of $f(t_i)$, we can write

$$f(t_i) = \sum_{j=1}^{N} a_j(t_i) f_j,$$

where $a_j(t_i) =< f(t_i), f_j >$. F_{snap} is a snapshot matrix whose columns are values of f at a sequence of time points. The complexity function in this extended case is defined as

$$c_o(F_{snap}) \triangleq \max_{t_i \in \mathbb{T}} \operatorname{card} \Big\{ a_j(t_i) \neq 0; 1 \leq j \leq N \Big\}.$$

The problem of optimal projection of F_{snap} onto $\mathcal{H}_1$ can be stated as follows: *given F_{snap} of complexity order $c_o(F_{snap})$, find F^1_{snap} with complexity order $c_o(F^1_{snap}) \leq c_o(F_{snap})$ such that $d_{mf}(F_{snap}, F^1_{snap})$ is minimal*. The solution of this problem is as follows. If the Fourier coefficients $\{a_j(t)\}$ are averaged over time sequences t_i and the averages are ordered as

$$\bar{a}^2_{i_1} \geq \bar{a}^2_{i_2} \geq \cdots \geq \bar{a}^2_{i_{c_o(F^1_{snap})}} \geq \cdots \geq \bar{a}^2_{i_N}, \quad (31)$$

where the bar denotes the average, then the optimal projection of F_{snap} onto $\mathcal{H}_1$ is given as

$$\hat{F}_{snap}(t_i) = \sum_{j=1}^{c_o(F^1_{snap})} a_{i_j}(t_i) f_{i_j}, \; 1 \leq i \leq n, \quad (32)$$

where

$$d_{mf}(F_{snap}, F^1_{snap}) = \sum_{j=c_o(F^1_{snap})+1}^{N} a^2_{i_j}.$$

From the results up to this point we see that the optimal projection problems are solved by ordering the Fourier coefficients or their averages. However, Fourier coefficients depend on the chosen basis functions. Therefore, the next problem is the determination of the optimal orthonormal basis (optimal in the sense of minimizing the misfit between F_{snap} and F^1_{snap} among all other candidate bases) $\{f_j\}$ from a snapshot matrix F_{snap} and then order the averages of Fourier coefficients to find the optimal projection for a given order. The solution steps of this optimal basis problem are as follows (See for example, (Holmes et al., 1996)):

- **step 1**: Construct the snapshot matrix from observations at a sequence of time points:

$$F_{snap} = \Big[f(t_1) \quad f(t_2) \cdots \quad f(t_n) \Big].$$

- **step 2**: From F_{snap} construct the correlation matrix C_{cor}:

$$C_{\text{cor}} = \frac{1}{N} F_{snap} F^T_{snap}.$$

- **step 3**: Solve the eigen-value problem

$$C_{\text{cor}} \Phi = \Phi \Lambda,$$

where $\Lambda = \operatorname{diag}\Big(\lambda_1, \lambda_2, \cdots, \lambda_N \Big) \succeq 0$ and Φ is an orthogonal matrix.

- **step 4**: Let ϕ_i be the i-th column of Φ, $i \in \mathbb{I}$. Then, $\{\phi_i\}_{i \in \mathbb{I}}$ is the optimal basis, which is called the *POD basis* in the literature.

REDUCED-ORDER MODELING OF BOREHOLE DYNAMICS USING POD BASIS

Letting $\mathcal{H}$ to be the $n_g + n_s + 1$-dimensional Euclidean space $\mathbb{R}^{n_g+n_s+1}$ containing $x_{sys}(t_k)$, we will determine a POD basis from a set of values of x_{sys} and then use it to obtain a reduced-order model for the typically large-scale system in Equation (28). The associated snapshot matrix is $F_{snap} = \Big[x_{sys}(t_1) \quad x_{sys}(t_2) \cdots \quad x_{sys}(t_n) \Big]$. Next, N eigenvalues are ordered and then the following sequence is constructed:

$$P_r = \frac{\sum_{i=1}^{r} \lambda_i}{\sum_{i=1}^{N} \lambda_i}, \; r = 1, \cdots, N. \quad (33)$$

Since eigen-values are positive, we have $0 < P_1 \leq P_2 \leq \cdots \leq P_N = 1$. The truncation degree r is chosen based on the value of P_r and it should be large enough to capture the system dynamics. Typically r is chosen such that $P_r \cong 0.99$ (Holmes et al., 1996). The reduced-order model is obtained using the state transformation $x_{sys} = \Phi_r x_{sys_r}$, where r is the truncation order in Equation (33), $\Phi_r \in \mathbb{R}^{(n_g+n_s+1)\times r}$ represents the first r columns of Φ and x_{sys_r} is the reduced-order system state vector. The reduced-order system is given as

$$x_{sys_r}(k+1) = A_{sys_r} x_{sys_r}(k) + B_{sys_r} u(k), \quad (34a)$$
$$y = C_{sys_r} x_{sys_r}(k) \quad (34b)$$

where $A_{sys_r} = (\Phi^T_r \Phi_r)^{-1} \Phi^T_r A_{sys} \Phi_r$, $B_{sys_r} = (\Phi^T_r \Phi_r)^{-1} \Phi^T_r B_{sys}$ and $C_{sys_r} = \Phi_r C_{sys}$.

REDUCED-ORDER MODEL VALIDATION

Next, we apply the POD approach to obtain a reduced-order model for the overall system presented by Equation (28) and then show its validation. To that end, we divide the grout region into 20 nodes and the soil region into 500 nodes. Other assumed parameter or

property values are given in Table 1. The time discretisation step size is 1 second. The system in Equation (28) is excited by a multi-sine random power input in the range of $[-500\ 500]$ W/m and the simulation period is 200 hours. Snapshots are created at every 500 seconds. The initial temperature for the field is assumed to be 10 °C. The eigen-value plot of C_{cor} is given in Figure 3 and based on it the selected order of the reduced-order model is 5.

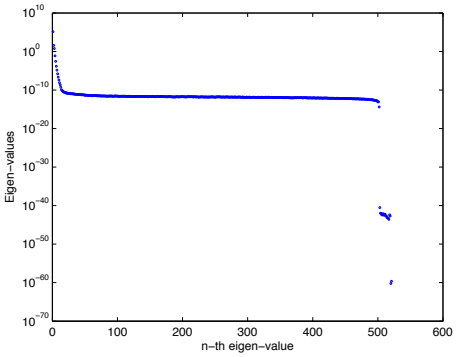

Figure 3: Eigen-values of correlation matrix.

For validation another multi-sine random power input in the range of $[-500\ 500]$ W/m is created and the circulating fluid mean-value temperatures are compared in Figure 4. As seen, the performance of the reduced-order model is very satisfactory. The thermal property values and the pipe size-related parameter values in Table 1 were taken from (**?**) where an equivalent analytical form of the large-scale model given by Equation (28) was derived in the Laplace-domain and experimentally validated.

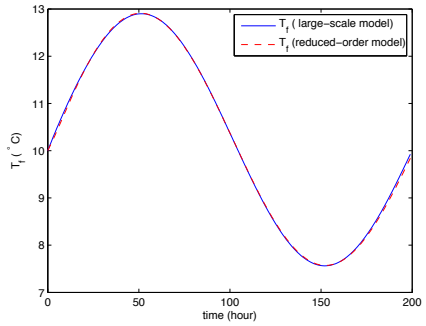

Figure 4: Validation of reduced-order model.

HEAT EXTRACTION and REJECTION CONTROL

The final objective is to design an LQR controller with Kalman filter state estimator based on the reduced-order model. The ratio of weight for penalizing tracking error over control input weight was selected to be 0.1. The controller is tested on the original large-scale model. Figure 5 and 6 show the control of heat extraction and rejection through tracking of set point values for T_f, respectively. The circulating fluid mean-value temperature set point is 3 °C for the heat extraction mode and 15 °C for heat rejection mode. The initial value of the circulating fluid mean-value temperature is taken equal to the undisturbed ground temperature, 10 °C. The high performance of controller is observed from the figures.

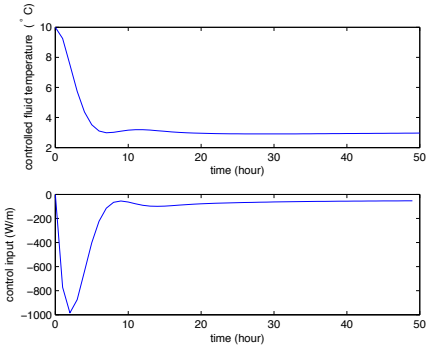

Figure 5: Set-point temperature control for heat extraction.

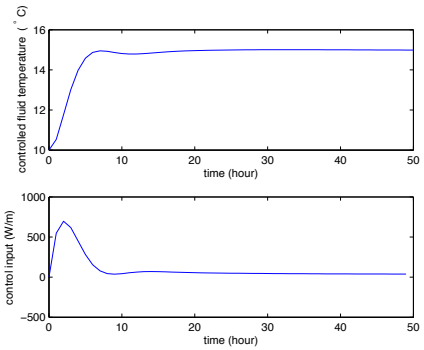

Figure 6: Set-point temperature control for heat rejection.

CONCLUSIONS AND FUTURE WORK

In this paper, a reduced-order control model for short-term prediction of circulating-fluid mean-value temperature in borehole heat exchangers was derived using a POD model order reduction technique. The main advantage of POD is that it is derived based on the governing mathematical equation of the system dynamics instead of using an input-output framework. As a result, it is possible to obtain a very low-order model with a good performance, as illustrated here. The borehole system was decomposed into 521 nodes or states where the first state corresponded to circulating fluid mean-value temperature. Hence, the order of the large-scale system describing the heat transfer dynamics was 521. The reduced-order model was fifth order, giving almost the same performance as the original one. Next, the reduced-order model was used to control the circulating fluid mean-value temperature set point values for heat extraction and rejection modes. The control algorithm was LQR with Kalman Filter for state-estimation. In fact, the developed reduced-order modeling approach can be used both for short-term and long-term simulation periods

by taking the snapshots over the corresponding time-periods but it is computationally efficient mainly for short-term periods since the simulation time step-size is 1 second. Therefore, it was used for mean-value temperature control of circulating fluid in short-term periods. The future extensions of the paper will be in the following directions:

- the large-scale model including both short-and long-term process dynamics will be obtained with a less number of nodes by considering a nonuniform grid size where the grid size increases from the grout region towards the far away soil region.
- the heat transfer in the vertical direction will be taken into account to obtain a 2-D large-scale model and the corresponding reduced-order model to be used for control purposes.
- by considering a set of borehole lengths, first a corresponding set of reduced-order 2-D borehole models and then a single model parameterized in terms of borehole length will be obtained from these set of reduced-order models. This parameterized model can be used to determine the optimal borehole length for a given purpose.
- the above concepts will be extended to borefield and to hybrid GHPs.

NOMENCLATURE

Table 1: Borehole system variables

Var.	Descrip.	Value
H	borehole length (m)	
α_g	grout diffis.(m^2/s)	4.8 $e-7$
α_s	soil diffis. (m^2/s)	1.6 $e-6$
k_g	grout conductivity (W/(mK))	1.5
k_s	soil conductivity (W/(mK))	3
k_p	pipe conductivity (W/(mK))	0.47
r_{fg}	grout reg. inner rad. (m)	0.26
r_{gs}	grout reg. outer rad. (m)	0.55
r_{p_i}	equival. pipe inner rad. (m)	0.26
r_{p_o}	equival. pipe outer rad. (m)	0.28
$r_\star$	soil reg. insulation rad. (m)	10
T_f	fluid mean temperature (K)	
$n_g(n_s)$	$\neq$ of grout (soil) nodes	20 (500)
$(\Delta r)_g$	discr. step size (grout) (m)	0.014
$(\Delta r)_s$	discr. step size (soil) (m)	0.019
Δt	time discr. step size (sec.)	1
c_f	fluid specific heat (J/(kgK))	4182
h_f	fluid convec. coeff. $(W/(m^2K))$	1700
ρ_f	fluid density $(kg/(m^3))$	1000

REFERENCES

Chiasson, A. D. 2007. *Simulation and Design of Hybrid Geothermal Heat Pump Systems*. Ph.d. thesis, University of Wyoming.

Cullin, J., S. J. D. 2010. Comparison of simulation-based design procedures for hybrid ground source heat pump systems. In *Proceedings of the 8th International Conference on System Simulation in Buildings, Liège, Belgium*.

EPBD 2010. Energy performance of buildings directive. Technical report, Directive 2010/31/UE.

Franke, R. 1998. *Integrierte dynamische Modellierung und Optimierung von Systemen mit saisonaler Wrmespeicherung*. VDI Verlag, Dsseldorf.

Holmes, P., Lumley, L., J., and Berkooz, G. 1996. *Turbulence, Coherence Structure, Dynamical Systems and Symmetry*. Cambridge University Press, Cambridge.

Javed, S. and Claesson, J. 2011. New analytical and numerical solutions for the short-term analysis of verical ground heat exchangers. *ASHRAE Transactions*, 117.

Kim, E. J., Roux, J. J., Bernier, M., and Caurent, O. 2011. Three-dimensionnal numerical modeling of vertical ground heat exchangers : Domain decomposition and state model reduction. *HVAC & R Research-Topical issue*, 17(6):912–927.

Monteyne, G., Vandersteen, G., Verhelst, C., and Helsen, L. 2011. On the use of laplace and warburg variables for heat diffusion modeling. In *0th International Conference on Environment and Electrical Engineering, Roma, Italy*.

Partenay, V., Riederer, P., Wurtz, E., and Salque, T. 2011. The influence of the borehole short-time response on ground source heat pump system. *Energy & Buildings*, 43:1280–1287.

Ridder, F. D., Diehl, M., Mulder, G., Desmedt, J., and Van, J. 2011. An optimal control algorithm for borehole thermal energy storage systems. *Energy and Buildings*, 43(10):2918–2925.

Scott, H. and Amanda, P. 2011. Effective design and operation of hybrid ground-source heat pumps: Three case studies. *Energy and Buildings*, 188(12):3497–3504.

Verhelst, C. 2012. *Model predictive control of hybrid ground coupled heat pump systems in office building*. Ph.d. thesis, Katholieke Universiteit Leuven.

Verhelst, C. and Helsen, L. 2011. Low-order state space models for borehole heat exchangers. *HVAC& R Research*, 17(6):928–947.

Yavuzturk, C. and Spitler, J. 1999. A short time step response factor model for vertical ground loop heat exchangers. *ASHRAE Transactions*, 105(2):475–485.